PUBLICATIONS OF THE ASTRONOMICAL SOCIETY OF THE PACIFIC, **117**:411–420, 2005 April

Laboratory Demonstration and Numerical Simulations of the Phase-Induced Amplitude Apodization

RAPHAEL GALICHER[1] AND OLIVIER GUYON

Subaru Telescope, 650 N. A'ohoku Place, Hilo, HI 96720; galicher@clipper.ens.fr, guyon@naoj.org

MASASHI OTSUBO AND HIROSHI SUTO

National Astronomical Observatory of Japan, Osawa 2-21-1, Mitaka, Tokyo 181-8588, Japan

AND

STEPHEN RIDGWAY

National Optical Astronomical Observatories, 950 North Cherry Street, Tucson, AZ 85719

Received 2005 January 5; accepted 2005 January 31; published 2005 March 21

ABSTRACT. Phase-induced amplitude apodization (PIAA) uses two aspheric optics to produce an achromatic apodization of an incoming beam by changing the geometrical distribution of the light in the pupil plane. Since this apodization is lossless, the sensitivity and angular resolution of the telescope are preserved, theoretically allowing efficient detection of Earth-size planets from space with a 2 m diameter optical telescope. In this paper, we report the first laboratory demonstration of imaging with a PIAA system. First, we show that the optics shapes computed by our algorithm produce an apodized collimated beam only by changing the geometrical distribution of the light and without losing light. We then present images of on- and off-axis point-spread functions and compare them with our numerical simulations.

1. INTRODUCTION

Since the discovery of the first extrasolar planet (Mayor & Queloz 1995), more than 100 Jupiter-size planets have been identified by radial velocity measurement of their host stars. Since the ultimate scientific goal of exoplanet studies is to evaluate the habitability of planets outside our own solar system, direct detection and low-resolution spectroscopy of Earth-size planets are highly desirable. The high contrast (10^{-10} in the visible) and small angular separation (typically less than 0.″1) of a Sun–Earth-like system needs to be overcome by an optical system allowing high dynamical range observations.

One solution to this problem is to use a high-performance coronagraph on a medium-size (2–8 m diameter) telescope in space. To eliminate the bright point-spread function (PSF) diffraction features (Airy rings), the amplitude function in the pupil plane can be changed (Jacquinot & Roizen-Dossier 1964). Unfortunately, classical pupil apodizations, such as shaped binary masks (Kasdin et al. 2003), have to remove most of the light of the pupil to produce a 10^{-10} contrast in the PSF, resulting in a poor sensitivity. Since the throughput is low on the edges of the pupil, these techniques also suffer from a poor angular resolution and consequently a large inner working angle (IWA $\geq 4\lambda/d$). Binary masks can reach contrasts sufficient to detect Earth-like planets at $4\lambda/d$ with a throughput of 25% (Vanderbei et al. 2003), which implies that they have to be used with a 6 m visible telescope to sample a reasonable number of stars. In 2003, Guyon (2003) suggested an alternative method to apodize a beam: phase-induced amplitude apodization (PIAA). This technique uses two aspheric mirrors to produce an achromatic apodization of an incoming beam by changing the geometrical distribution of the light (Guyon 2003; Traub & Vanderbei 2003; Guyon et al. 2005). The PIAA optics redistribute the light intensity in the pupil plane to produce the desired apodization profile without introducing phase errors for on-axis sources. Unlike classical apodization, PIAA does not absorb any light of the incoming beam, which means that the angular resolution of the telescope (about λ/d) and its sensitivity are preserved. Therefore, a PIAA system performs as well as a classical apodizer on a telescope 2 to 3 times smaller (Guyon 2003; Guyon et al. 2005). In this paper, we report the first experimental results obtained with a PIAA system using aspheric lenses instead of mirrors. The PIAA lens manufacturing process is described in § 2. We present in § 3 the optical layout of the experiment for pupil plane and focal plane imaging. The results of the laboratory experiment are shown in § 4, in which pupil plane and focal plane images acquired with our setup are compared to numerical simulations.

[1] Current address: École Normale Supérieure, 45 Rue d'Ulm, Paris 75005, France.

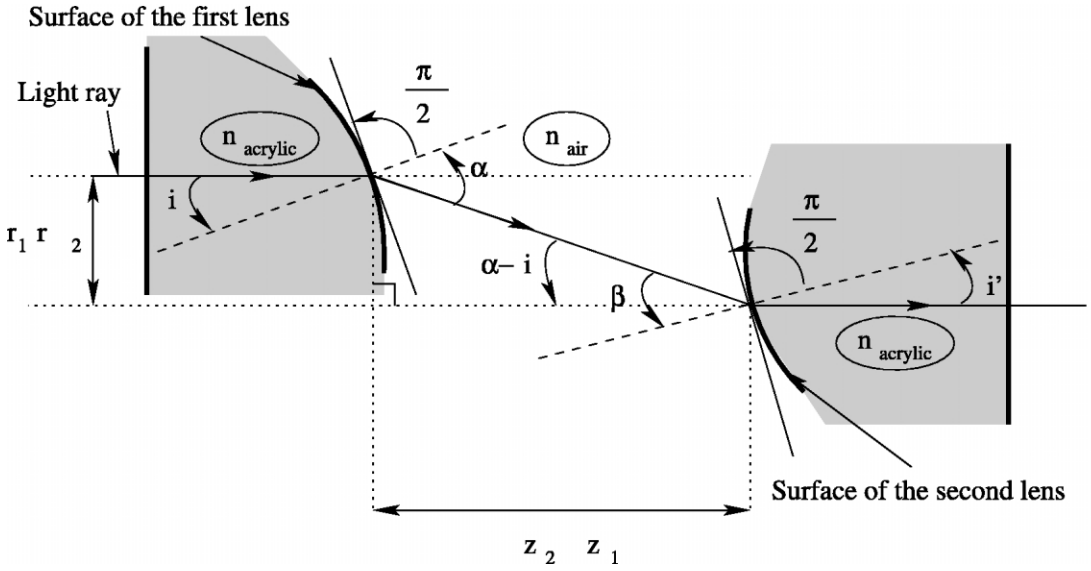

FIG. 1.—Path of light ray through PIAA lenses.

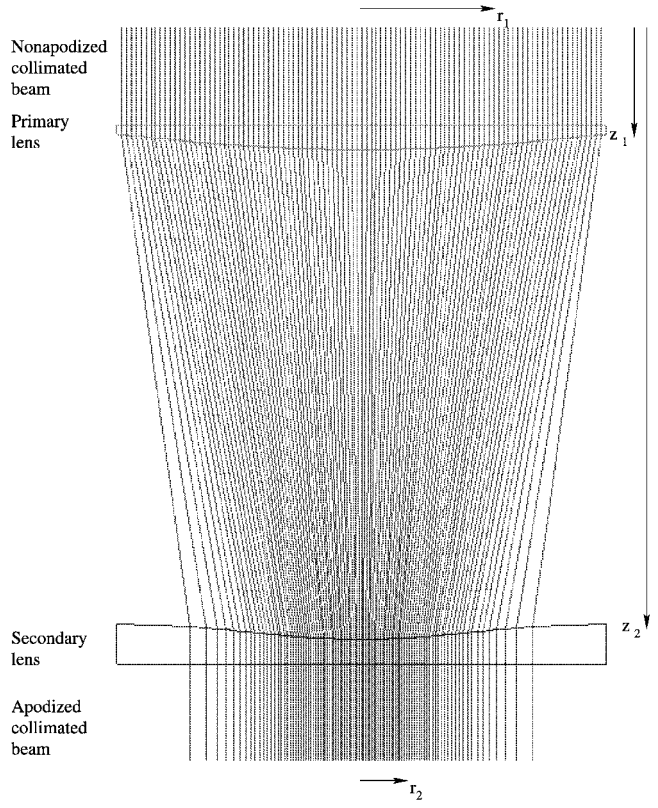

FIG. 2.—Lens shapes computed by our algorithm and path of light rays. Horizontal and vertical scales are different (in the real system, the distance between the lenses is equal to 4 times the beam diameter).

2. OPTICS MANUFACTURING

2.1. Optics Shapes

PIAA lens shapes depend on the desired apodization function. We use the geometrical transformation of the light inside the PIAA to obtain a differential equation, as was done in a previous paper (Guyon 2003) for mirrors. Figure 1 shows notations used to establish the differential equation. Here r_1, r_2, z_1, and z_2 are, respectively, the distance from the optical axis in the input and output beams and the shapes of the first and second lenses, as shown in Figure 2. The variables $n_{\rm air}$ and $n_{\rm acrylic}$ are the refractive indexes of the air and of the acrylic in which the lenses have been polished. The light rays are refracted by the surface of each lens:

$$n_{\rm air}\ \sin(i) = n_{\rm acrylic}\ \sin(\alpha), \tag{1}$$

$$n_{\rm air}\ \sin(i') = n_{\rm acrylic}\ \sin(\beta). \tag{2}$$

Using the two trigonometric equations

$$\sin(\alpha) = \sin(\alpha - i)\cos(i) + \sin(i)\cos(\alpha - i), \tag{3}$$

$$\sin(\beta) = \sin(\beta - i')\cos(i') + \sin(i')\cos(\beta - i'), \tag{4}$$

and the geometrical considerations in Figure 1,

$$\sin(\alpha) = \frac{(r_1 - r_2)\cos(i) + [z_2(r_2) - z_1(r_1)]\sin(i)}{\sqrt{(r_1 - r_2)^2 + [z_2(r_2) - z_1(r_1)]^2}}, \tag{5}$$

$$\sin(\beta) = \frac{(r_1 - r_2)\cos(i') + [z_2(r_2) - z_1(r_1)]\sin(i')}{\sqrt{(r_1 - r_2)^2 + [z_2(r_2) - z_1(r_1)]^2}}, \tag{6}$$

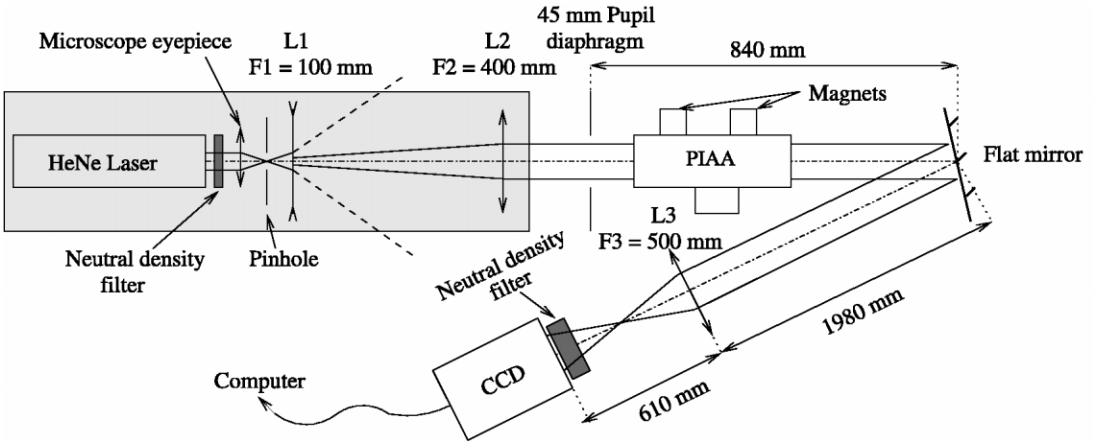

FIG. 3.—Configuration of the optical bench for pupil image acquisition.

Equations (1) and (5) (respectively eqs. [2] and [6]) yield equation (7) (respectively eq. [8]):

$$\tan(i) = \frac{A}{(n_{\rm acrylic}/n_{\rm air})\sqrt{B^2 + A^2} - B}, \tag{7}$$

$$\tan(i') = \frac{A}{(n_{\rm acrylic}/n_{\rm air})\sqrt{B^2 + A^2} - B}, \tag{8}$$

where $A = r_1 - r_2$ and $B = z_2(r_2) - z_1(r_1)$.

The slopes for the first and second lens are respectively

$$\frac{dz_1}{dr_1} = \tan(i), \tag{9}$$

$$\frac{dz_2}{dr_2} = \tan(i'). \tag{10}$$

Finally, by using equations (7)–(10), we obtain the following differential equation:

$$\frac{dz_1}{dr_1} = \frac{dz_2}{dr_2} = \frac{A}{(n_{\rm acrylic}/n_{\rm air})\sqrt{B^2 + A^2} - B}. \tag{11}$$

This differential equation produces the optics shapes shown in Figure 2, where light rays have been drawn. The first part of the equation guarantees that the output beam is collimated if the incoming beam is collimated (no phase aberrations for an on-axis source).

2.2. Polishing the PIAA Lenses

Each lens was polished out of 10 mm thick, 50 mm diameter acrylic substrate with a high-accuracy diamond-turning machine. In this on-axis system, the optics surfaces are rotationally symmetric and therefore defined by a radial profile. Special attention was given to the outer edge of the first PIAA lens (where the incoming beam enters the system), since its slope changes rapidly with distance to the optical axis. This feature is essential to "spread" the light into the extended wings of the apodized beam.

3. EXPERIMENT SETUP

3.1. Description of the Different Optical Configurations

We used two different optical configurations to acquire pupil and PSF images. The experiment setups are respectively shown in Figures 3 and 4. The diameter of the pupil diaphragm is about 45 mm. The PIAA unit, described in § 3.2, is composed of two aspheric lenses, and magnets mark its exact position to avoid having to realign the unit relative to the bench each time it is inserted in the beam. The source is a HeNe laser (632.8 nm). The beam is concentrated by a microscope eyepiece on a pinhole. Pasted to this pinhole, a diverging lens spreads the light to create a nonapodized beam, which is collimated by a converging lens.

For the pupil image configuration, a flat mirror folds the beam because of the lack of space on the optical bench, and a 500 mm converging lens L3 is used to produce the image of the pupil plane (pupil diaphragm) on the detector of the CCD camera.

For the PSF image configuration, a tip-tilt adjustable flat mirror simulates off-axis sources. The converging lenses L1 (750 mm focal length) and L2 (200 mm focal length) are used to produce a well-sampled PSF on the CCD camera. A neutral-density filter is used to avoid saturation of the detector.

3.2. The PIAA Prototype Unit

If a nonapodized collimated beam enters the PIAA, an apodized collimated beam is produced without losing any light. The new light intensity distribution is mostly produced by the first mirror, while the second mirror is shaped to correct the phase

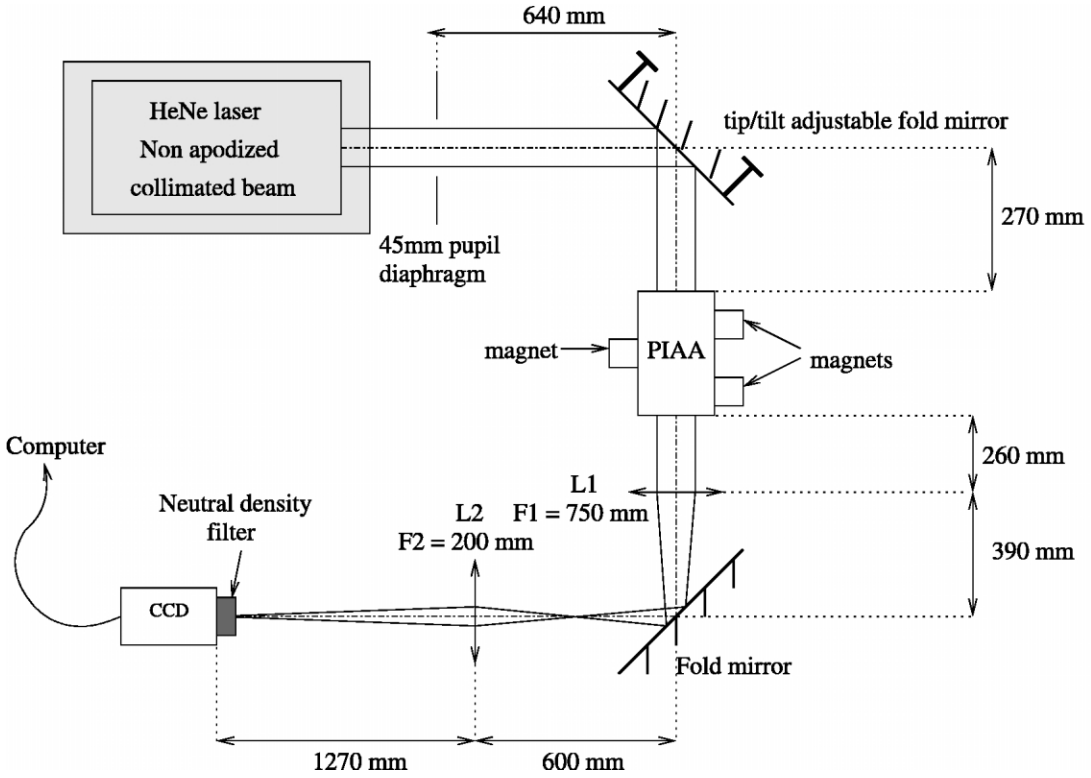

FIG. 4.—Configuration of the optical bench for focal image acquisition.

aberrations introduced by the first mirror. The two mirrors are aspheric, and the performance of the system relies on the accurate polishing of their surfaces. The principle is the same when the two mirrors are replaced by two lenses, as in the current prototype. The first lens mostly deflects the light, and the second one corrects the phase errors to produce a collimated beam. If lenses are used, the technique is chromatic, whereas it is achromatic with mirrors.

The prototype unit is shown in Figure 5. It uses two aspheric acrylic lenses. The optics are manually aligned to maximize PSF contrast. We used a shearing interferometer in the output beam of the PIAA to verify beam quality. As seen in Figure 6, the beam is quite well collimated (if it were not, interference fringes would be very tight) but contains phase errors due to the polishing lens defects.

4. LABORATORY RESULTS AND NUMERICAL SIMULATIONS

4.1. Image Acquisition and Processing

All images were taken with a 512 × 512 pixel CCD (20 μm pixels) with flat-fielding and dark-frame subtraction. The flat field was acquired by placing a light source in front of the camera, with no optics between the light source and the camera. The sole purpose of this flat-field frame was to correct for pixel-to-pixel variations in sensitivity within the camera. A neutral-density filter was used to avoid saturation. Incremental exposure times were combined to produce high dynamical range focal plane and pupil plane images. Radial profiles have been computed using both average and the median of the values of pixels at a common distance from the PSF center. We used the median measure to mitigate the effects of bright localized speckles due to optical defects in the lenses.

4.2. Pupil Apodization

4.2.1. Pupil Images

Figure 7 shows pupil images without (*left*) and with (*right*) the PIAA unit. The concentric rings seen with the PIAA are due to the circular polishing defects on the lenses produced by diamond turning.

To illustrate how the PIAA apodizes a beam, we put a striped mask in the input beam (Fig. 8). Without the PIAA, the horizontal straight bars of the mask can be seen undistorted, while the same bars become curved through the PIAA. This illustrates how the PIAA squeezes the light near the center of the pupil and spreads it near the edges.

4.2.2. Experimental Pupil Plane Intensity Radial Profiles

Using the method explained in § 4.1, we obtained pupil plane intensity radial profiles with and without the PIAA (Fig. 9). Polishing defects in the lenses are circular and can focus the

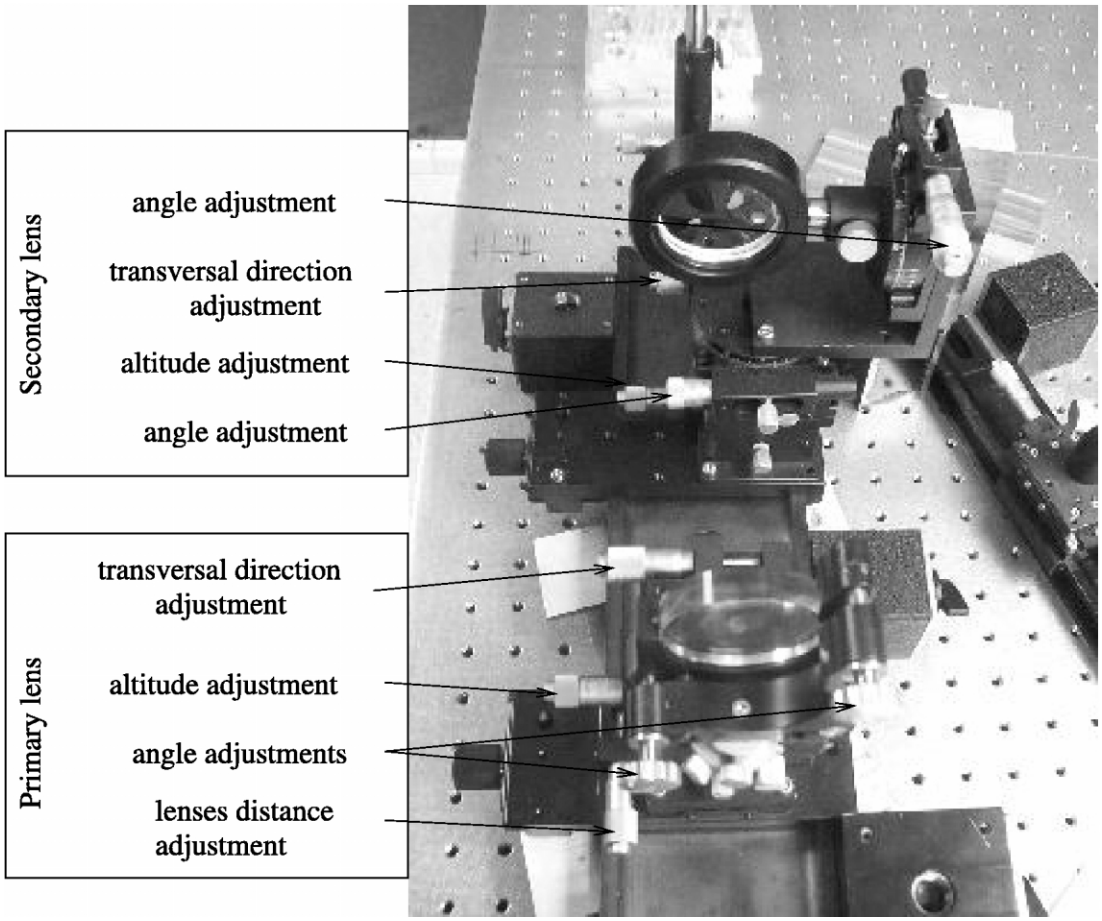

FIG. 5.—Image of the PIAA prototype unit. It is composed of two aspheric acrylic lenses. Each lens can be translated along three axes. Two other axes per lens enable us to adjust the angle between each lens and the beam. Finally, a manual actuator is used to adjust the distance between the two lenses.

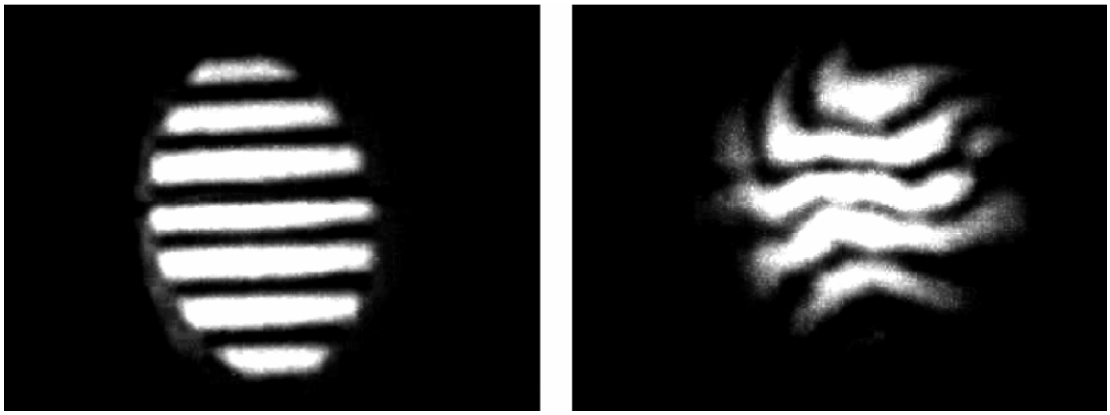

FIG. 6.—Images of the screen of a shearing interferometer used on the beam without (*left*) and with (*right*) the PIAA. Without the PIAA, the beam is well collimated and the wave front is flat. The wave-front errors with the PIAA are due to the polishing lenses defects, which introduce phase errors.

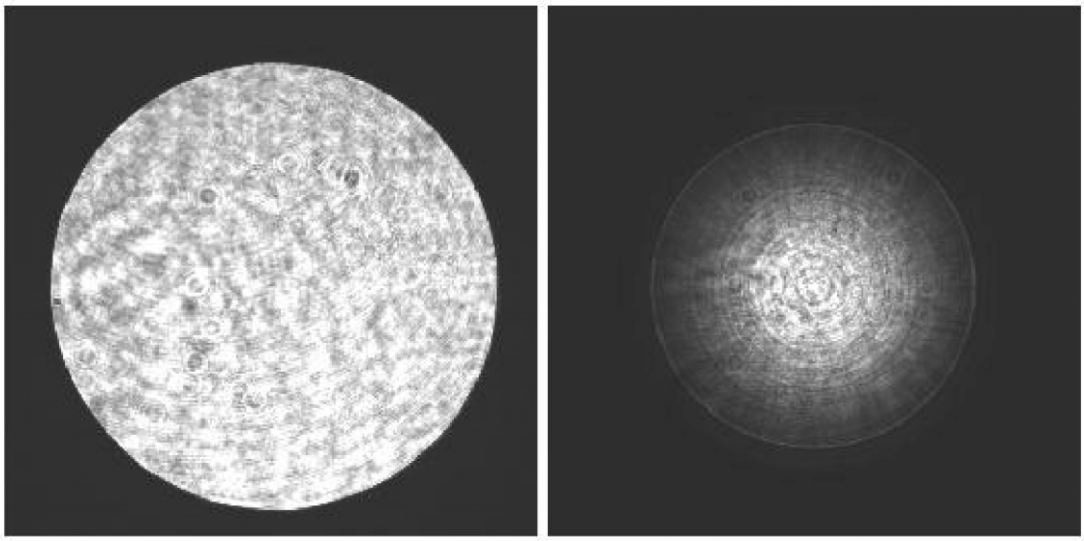

FIG. 7.—Pupil images without (*left*) and with (*right*) the PIAA. Without the unit, the pupil is quite uniformly lit. With the PIAA, the pupil is apodized as expected. The thin concentric rings are due to the circular polishing defects of the PIAA lenses.

light to the center of the pupil or create bright, thin circles, as seen in Figures 7 and 9. Since the circular "grooves" produced by diamond turning can be narrow, these features are sharp, and are modified by Fresnel propagation over short distances: the exact position an intensity of these "rings" varies along the beam. The edge of the beam is also a source of both polishing errors (because of the difficulty of polishing the sharp bend at the outer edge of the first lens) and Fresnel diffraction.

As expected, the PIAA is able to transform a nonapodized collimated beam into an apodized collimated beam only by changing the geometrical distribution of the light and without losing any light (the total flux is the same for both profiles).

4.3. Experimental and Simulated PSFs

4.3.1. On-Axis PSFs

The normalized radial profiles of experimental PSFs obtained without and with the PIAA are shown in Figure 10. Without the PIAA, the PSF is very close to the Airy function. Because of the finite spatial sampling by the CCD pixel and the finite size of the light source, the light intensity in the dark rings is not 0. The peak intensity of the first bright ring at $1.64\lambda/d$ is 1.62% of the central peak brightness. With the PIAA, no rings are visible and the main diffraction peak is widened. The PIAA prototype is not able to remove the first ring of the Airy function and produces a worse PSF than the one obtained without the PIAA. This is mainly due to the polishing defects of the lenses (see § 4.2.1). To illustrate that the polishing defects are the main limitation of the PIAA prototype, we simulated a PIAA producing the apodization function measured with our prototype, but without any phase errors in the pupil plane. The results are shown in Figure 10. While simulated and experimental PSFs are quite similar without the PIAA, the PSF produced by the simulated PIAA (without any phase errors in the pupil plane) is much better than the one obtained without the PIAA. The simulated PIAA strongly attenuates the first Airy ring. If the central peak brightness is normalized to 1, the value of the first bright ring is 1.63×10^{-2} at $1.64\lambda/d$ without the PIAA. At the same distance ($1.64\lambda/d$), the brightness is 2.70×10^{-4} with the simulated PIAA, instead of 5.50×10^{-2} with the PIAA prototype. This demonstrates that the polishing defects of the lenses are the main limitation of the PIAA prototype (they introduce large phase errors across the pupil plane). To correct these phase errors, we could use a deformable mirror, which would enable us to obtain the PSF of the simulated PIAA. In a perfectly polished PIAA system, some phase errors may also be produced by Fresnel propagation, since this effect was not taken into account to compute the shape of the lenses. Unlike the phase errors shown in Figure 11, these errors are symmetric by rotation in the pupil plane, have a larger amplitude at the edge of the beam, and have a higher spatial frequency than those measured. The phase errors seen in Figure 11 are therefore dominated by errors in the polishing of the lenses, which introduces optical path-length difference variations across the beam. Significantly better optics or numerical simulations would be required to estimate the effect of Fresnel propagation on the system.

4.3.2. Off-Axis PSFs

The first fold mirror was used to move the source off-axis (Fig. 4). First, note in Figures 11 and 12 that the PSF produced

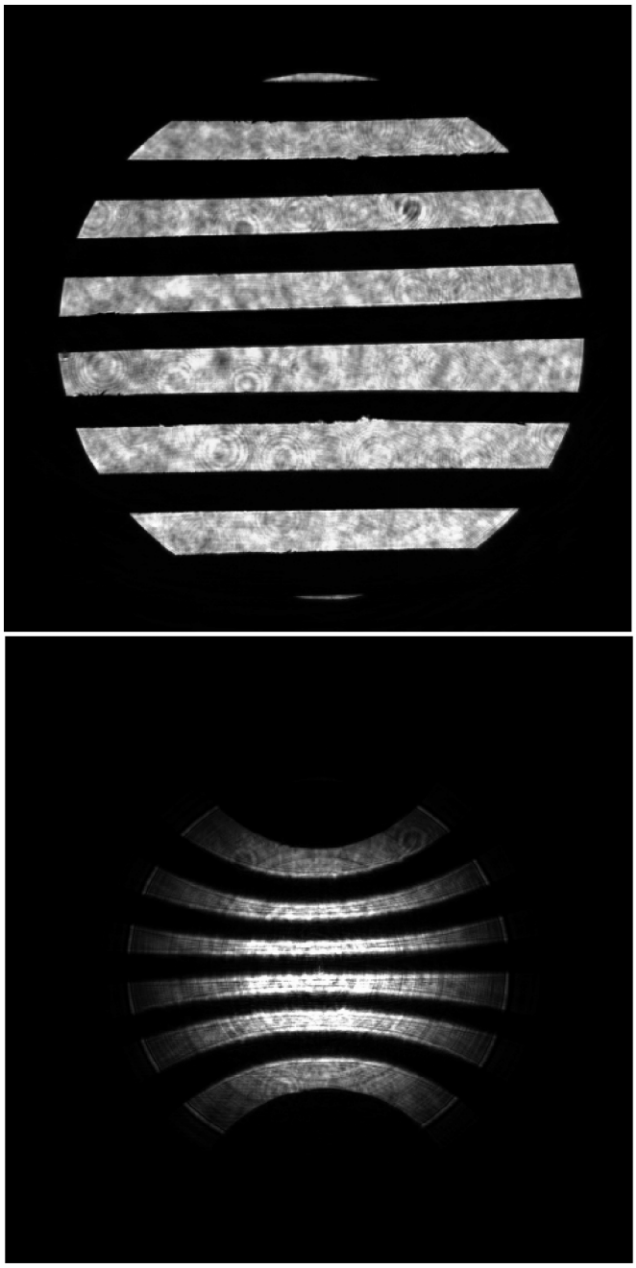

FIG. 8.—Pupil images of a striped mask without (*top*) and with (*bottom*) the PIAA. The images illustrate how the PIAA apodizes the beam by changing the geometrical distribution of the light in the pupil plane.

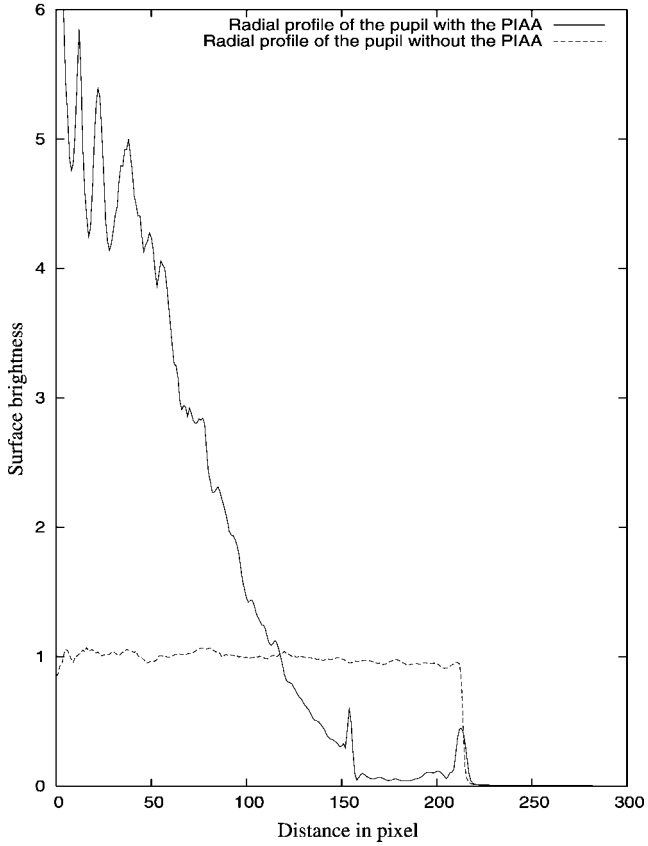

FIG. 9.—Intensity radial profiles in the pupil plane without and with the PIAA. The central intensity peak (brightness is 11.76) and the bright rings in the apodization profile are due to defects of the diamond-turned lenses.

by the PIAA is not translation invariant. The PIAA redistributes both the amplitude and the phase of the incoming beam. Through the PIAA, an off-axis source produces a distorted wave front, as seen in Figure 11, taken from Guyon et al. (2005). In this figure, for which the apodization profile is slightly different than the one obtained in our experiment, the top image is a simulated map of the output phase of the PIAA for a $10\lambda/d$ off-axis source, and the bottom image is the corresponding PSF. We also show the correspondence between different areas of the PSF and of the phase map in the output pupil of the PIAA. For instance, the center of the pupil, where the phase slope is maximum, corresponds to the brightest peak in the focal plane. The value of the slope in the center of the output pupil of the PIAA is different from the value of the slope in the center of the entrance pupil. This is a result of the geometrical redistribution of the pupil phase induced by the PIAA. At the center of the beam, the PIAA amplifies phase slopes and therefore magnifies the plate scale (Guyon 2003; Traub & Vanderbei 2003; Guyon et al. 2005). If the apodization function is smooth, the magnification factor can be approximated by $\sqrt{I_{\max}}$, where $I_{\max}$ is the ratio of the central intensity of the output and entrance pupils (Guyon et al. 2005).

We used focal plane images to measure the focal plane plate scale. PSFs were acquired with and without the PIAA, with the same fold mirror tilt. We measured the distance between the brightest point of the PSF and the optical axis for several fold mirror tilts. This allowed us to compute the ratio between the focal plane plate scales with and without the

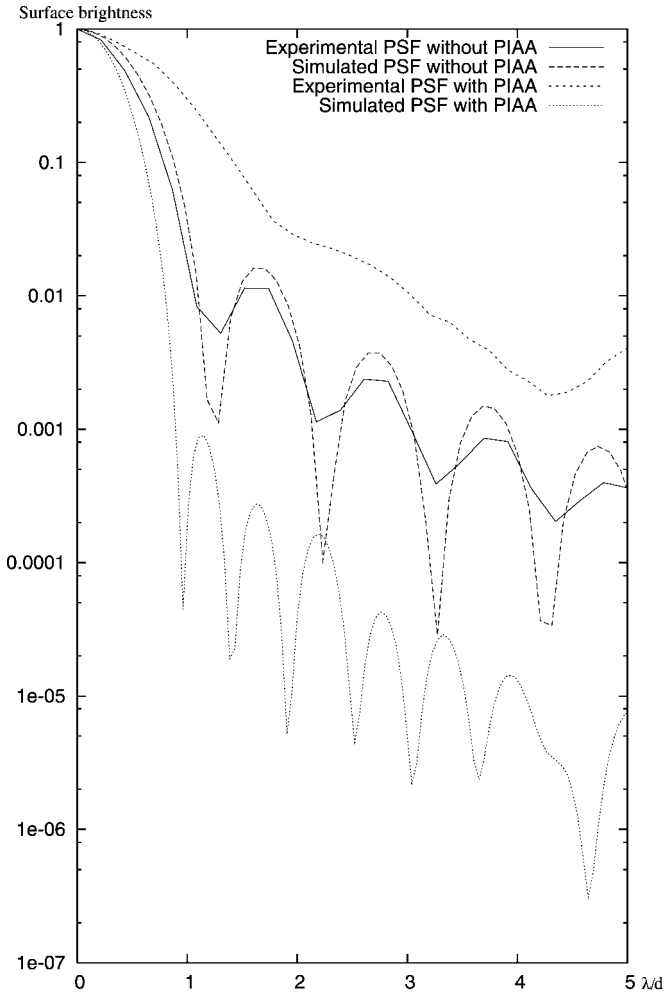

FIG. 10.—Normalized intensity radial profiles of the experimental and simulated on-axis PSFs without and with the PIAA. Without the PIAA, simulated and experimental PSFs are quite close, and the brightness of the first bright ring is $1.62.10^{-2}$ at $1.64\lambda/d$. At the same distance, the brightness is 2.70×10^{-4} with the simulated PIAA (see text for details) and 5.50×10^{-2} with the PIAA prototype.

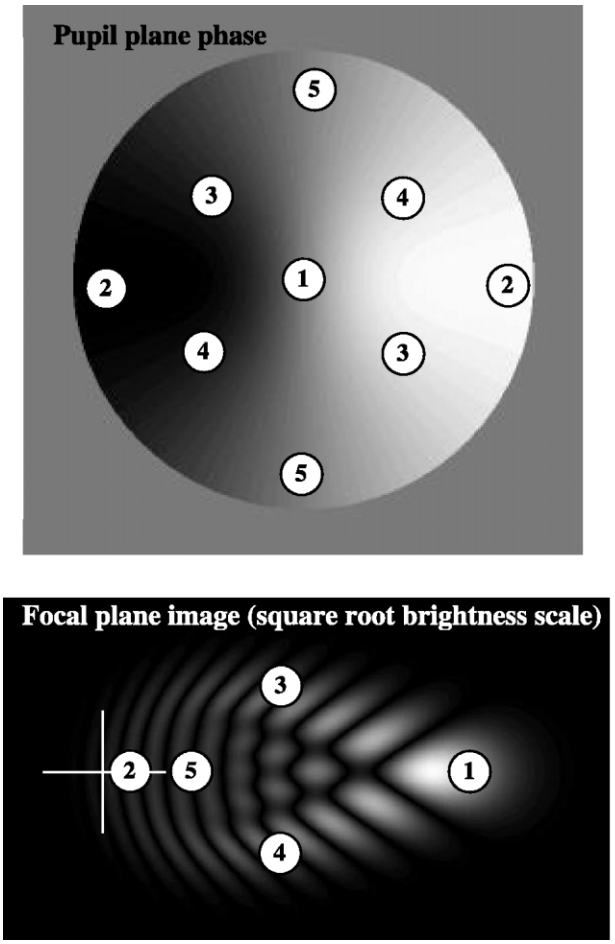

FIG. 11.—Simulated phase map of the PIAA output beam for a $10\lambda/d$ off-axis source (*top*) and the corresponding PSF (*bottom*). Numbers are used to show how PSF structures can be identified in the pupil plane. For instance, the phase slope at the center of the pupil gives the position of the brightest point of the PSF (point number 1). Reprinted with permission from Fig. 5 of Guyon et al. (2005).

PIAA. The plate scale without the PIAA was measured on the experimental image by fitting with a theoretical Airy pattern. As seen in Figure 12, the experimental (*left*) and simulated (*right*) PSFs show similar structures. Differences are due to the polishing defects of the lenses, which introduce phase errors in the PIAA output beam.

5. CONCLUSION

The first laboratory experiment of the phase-induced amplitude apodization demonstrated the following points:

1. The PIAA prototype transforms a nonapodized collimated beam into an apodized collimated beam with a 100% throughput (Figs. 7 and 9). This apodization is done only by changing the geometrical distribution of the light (Fig. 8).

2. No phase error other than that expected from the polishing defects of the lenses was seen for an on-axis source: the PIAA output beam is collimated (see Fig. 6).

3. We have validated our algorithm to compute the PIAA optics shapes shown in Figure 2.

4. Off-axis PSFs obtained in the laboratory are in good agreement with the results of our simulations (Fig. 12).

The surface accuracy of our diamond-turned lenses did not, however, allow us to obtain a high-contrast on-axis PSF. Even with perfect lenses, chromaticity of the refraction index would be incompatible with the high-contrast/wide spectral bandwidth requirement of a coronagraph suitable for direct detection of Earth-size planets. Since geometrical optics (ray-

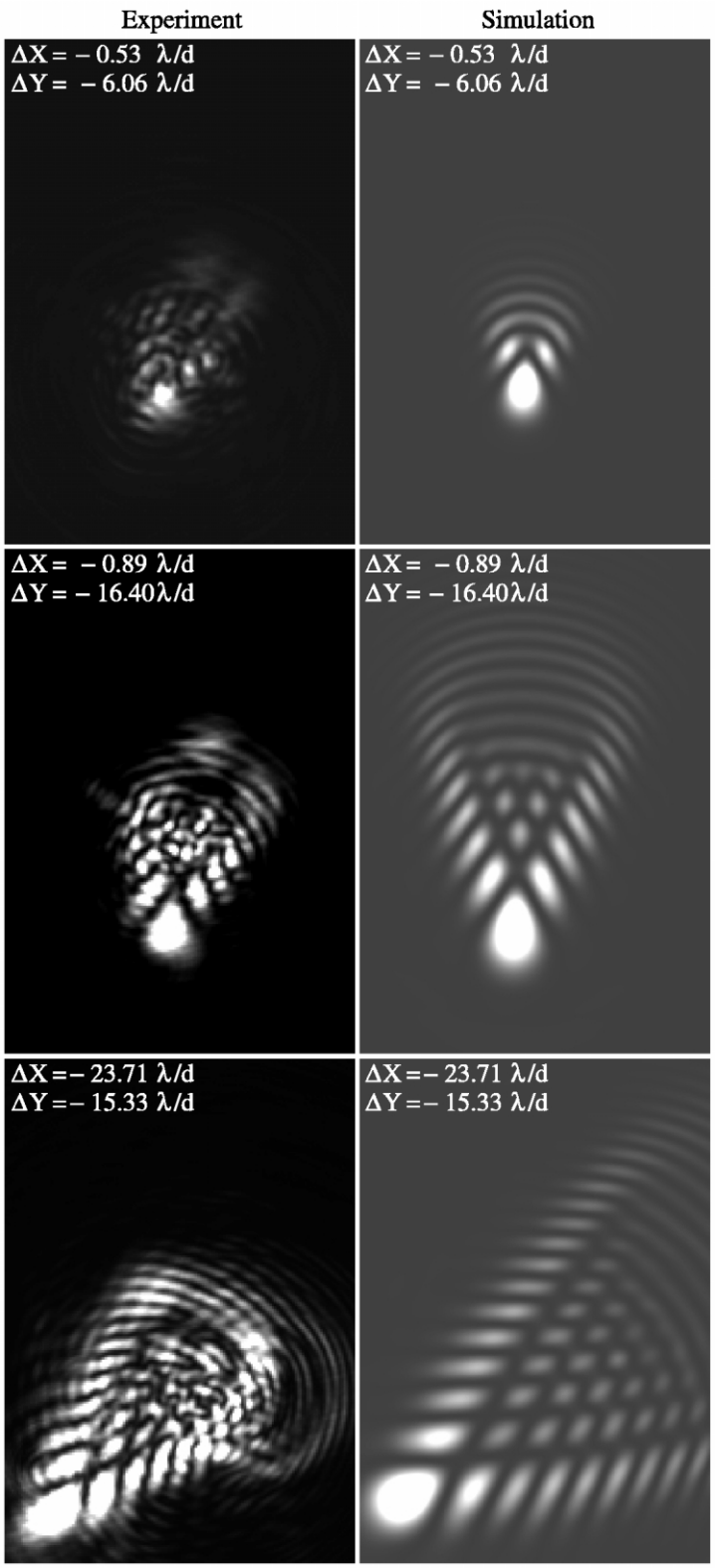

FIG. 12.—Experimental (*left column*) and simulated (*right column*) PSFs corresponding to three different distances of the source-to-optics axis. The two first images have been obtained by moving the source along only one axis, and the third image is a combination of motions along the two axes. Scales of experimental and simulated images are slightly different.

tracing) theory is used to design the PIAA system, higher quality optics would be useful to measure or put an upper limit to diffractive effects in the apodizing system (Fresnel propagation). These effects could also be modeled by numerical simulations. We are therefore planning another laboratory experiment with higher quality reflective optics and wave front control. This next step will include a focal plane occulting mask and a second set of optics aimed at removing the off-axis PSF aberrations produced by the first set (Guyon et al. 2005).

A lens-based PIAA unit could, however, be successfully used for a ground-based coronagraph or as the second-stage corrective optics of a PIAAC (Guyon et al. 2005). In both cases, small amounts of chromaticity can be tolerated.

This work was carried out with the support of the National Astronomical Observatory of Japan and JPL for the Development of Technologies for the Terrestrial Planet Finder Mission (contract numbers 1254445 and 1257767).

REFERENCES

Guyon, O. 2003, A&A, 404, 379
Guyon, O., Pluzhnik, E. A., Galicher, R., Martinache, F., Ridgway, S. T., & Woodruff, R. A. 2005, ApJ, 622, 744
Jacquinot, P., & Roizen-Dossier, B. 1964, Prog. Opt., 3, 29
Kasdin, N. J., Vanderbei, R. J., Spergel, D. N., & Littman, M. G. 2003, ApJ, 582, 1147
Mayor, M. & Queloz, D. 1995, Nature, 378, 355
Traub, W. A., & Vanderbei, R. J. 2003, ApJ, 599, 695
Vanderbei, R. J., Kasdin, N. J., & Spergel, D. N. 2003, ApJ, 590, 593